Research Square

Preprints are preliminary reports that have not undergone peer review.
They should not be considered conclusive, used to inform clinical practice,
or referenced by the media as validated information.

[^{18}F]NaF PET Radiomics and Coronary Calcium Score Progression: Associations Beyond Baseline Calcium Score and TBR

Suning Li

juliet.li@health.wa.gov.au

The University of Western Australia https://orcid.org/0009-0002-0007-9401

Jake Kendrick
The University of Western Australia

Martin A. Ebert
The University of Western Australia

Ghulam Mubashar Hassan
The University of Western Australia

Nathaniel Barry
Sir Charles Gairdner Hospital

Sing Ching Lee
Royal Perth Hospital

Roslyn J. Francis
The University of Western Australia

Jamie W. Bellinge
Fiona Stanley Hospital

Carl Schultz
Royal Perth Hospital

Research Article

Keywords: [18F]NaF PET, Coronary Calcification, Radiomics, Diabetes Mellitus, Cardiovascular Risk Stratification

Posted Date: October 18th, 2026

DOI: https://doi.org/10.21203/rs.3.rs-11165606/v1

License: This work is licensed under a Creative Commons Attribution 4.0 International License.
Read Full License

Abstract

Background:

[^{18}F]NaF positron emission tomography (PET) can quantify coronary calcification activity before coronary calcium score (CCS) progression, which is a surrogate measure of cardiovascular disease risk. It remains uncertain whether advanced PET quantification, including radiomics, improves prediction of CCS progression.

Participants with type 2 diabetes underwent baseline [^{18}F]NaF PET/CT, baseline CCS and a follow-up CCS after 2 years. CCS progression was evaluated on a per-patient and a per-artery level. [^{18}F]NaF activity was evaluated using the TBR_{max}, and radiomics features. Logistic regression models were used to determine the features most associated with CCS progression.

Results:

In total, 91 participants (median age [interquartile range]: 66 [60 – 70], 71.4% male) were examined. In total, 68 patients (74.7%) demonstrated CCS progression. Clinical variables and baseline CCS discriminated CCS progressors and non-progressors modestly (AUC 0.72, 95% CI 0.55–0.86). The TBR_{max} demonstrated good discrimination (AUC 0.83, 95% CI 0.73–0.92), while multi-feature radiomics models achieved the highest discrimination performance (AUC 0.90, 95% CI 0.80–0.97). A total of 211 coronary arteries (58.0%) demonstrated CCS progression. The combined CCS and TBR_{max} model discriminated CCS progressors and non-progressors modestly (AUC of 0.67, 95% CI 0.60–0.73), while the multi-feature radiomics demonstrated good discrimination (AUC 0.77, 95% CI: 0.70–0.84).

Conclusions:

[^{18}F]NaF PET radiomics improves prediction of CCS progression compared with baseline CCS, clinical features, and the TBR_{max}.

Key Points

- **Question:** Can coronary [18F]NaF PET radiomics identify patients with type 2 diabetes likely to develop coronary calcium score progression before macroscopic calcification advances?
- **Findings**: Model discrimination improved from clinical variables plus baseline CCS (AUC 0.72) to [^{18}F]NaF TBR_{max} (0.83), with multi-feature [^{18}F]NaF PET radiomics performing best (0.90).
- **Relevance**: Radiomics analyses can be reliably performed on coronary PET studies and may be a reliable quantitative metric in future studies using coronary PET as a prognostic tool, or as an endpoint for trials of novel anti-atherosclerotic therapies.

Background

The computed tomography (CT) coronary calcium score (CCS) remains a highly effective non-invasive technique for cardiovascular disease (CVD) risk stratification in asymptomatic individuals [1]. As a reliable indicator of coronary atherosclerotic burden, serial assessment of CCS enables the estimation of disease progression and provides incremental risk stratification information beyond baseline CT CCS alone [2]. However, the change in CT CCS can only be evaluated after irreversible calcifications have developed [2]. Improved imaging techniques are needed to identify early calcification activity before macroscopic disease is established.

[^{18}F]NaF positron emission tomography (PET) is a unique molecular imaging modality that can detect active coronary microcalcification activity (CMA) within the vasculature before they manifest as macrocalcific deposits detectable by CT [3]. Atherosclerotic plaques with increased CMA demonstrate other microscopic features of active atherosclerotic disease [4, 5]. In cohorts of people with diabetes, [^{18}F]NaF has demonstrated independent predictive capabilities for rate of vascular calcification progression [6, 7], and the burden of CMA has been shown to be an independent predictor of cardiac death or non-fatal myocardial infarction [8].

PET imaging of the coronary arteries is an evolving technique to examine molecular components of atherosclerosis. With advances in the sensitivity of PET camera technologies [9], motion correction software [10] and emerging radiotracers for coronary artery disease imaging [11, 12], there is an ongoing need to optimise approaches to coronary PET analysis and molecular disease-specific quantification techniques.

Current approaches to coronary PET quantification use simple uptake metrics, such as single measure standardised uptake value (SUV), tissue-to-background ratio, or whole coronary vessel activity measures [13]. PET radiomics approaches quantify voxel-level intensity distributions and texture patterns [14]. These allow for a more detailed characterisation of PET images, integrating spatial and intensity information, some of which may be imperceptible to visual assessment [15]. These approaches have demonstrated reproducibility [16] though, in the context of CCS progression or coronary-specific PET analyses, their clinical relevance remains unknown.

Therefore, in a cohort of individuals without a history of coronary heart disease but with established coronary artery calcification, we aimed to evaluate the predictive value of [^{18}F]NaF PET radiomics, including traditional measures such as the TBR_{max}, for CCS progression, and to compare performance with baseline CCS and clinical measurements.

Material and Methods

Study design

This study is a post-hoc analysis of the VikCoVac trial [17] that was a double-blind 2x2 factorial placebo-controlled trial of the effect of vitamin K1 and colchicine on arterial calcification activity, as measured with [^{18}F]NaF PET. The trial is registered under ACTRN12616000024448 in the Australian New Zealand Clinical Trials Registry and approved by the Royal Perth Hospital Human Research Ethics Committee (REG14-095). The study cohort and detailed inclusion and exclusion criteria have been previously described [17]. In brief, individuals aged 50 to 80 with type-1 or type-2 diabetes, and without a history of clinical coronary heart disease, were enrolled between August 2015 and May 2018. All individuals underwent CT CCS screening and those with a CCS above 10, along with ten individuals with a CCS of zero, were invited to participate in the trial [6, 17]. Written informed consent was obtained from all participants.

Baseline assessment, imaging and follow-up

At baseline, all individuals were reviewed clinically, and had their medical history, medication history and CVD risk scores assessed. Bloods samples were taken for lipid analyses and HbA1%. Participants underwent electrocardiogram (ECG)-gated CT CCS imaging using either a Philips iCT system (128 detector rows, 256 slices, 120 kV, 40 mAs) or a Siemens Definition AS+ scanner (64 detector rows, 128 slices, 120 kV, 60 mAs). Shortly after enrolment, subjects underwent [^{18}F]NaF PET/CT imaging on a Siemens mCT64 PET/CT scanner following intravenous administration of 250 MBq [^{18}F]NaF and a 60-minute rest period. Participants were treated with oral beta blocker or ivabradine therapy to target a heart rate ≤ 60 bpm. Two years after the trial's conclusion, participants were recruited for repeat medical review and CT CCS.

CCS calculation and image processing

The CCS was calculated using the Agatston method, for each coronary artery at both timepoints, using Osirix MD (version 9.5.1, Pixmeo, Switzerland) [18]. [^{18}F]NaF PET coronary images were manually segmented using a customised workflow in MIM (version 6.8.3, MIM Software, Inc.) from diastolic phase ECG-gated PET studies co-registered with CT CCS images. The segmentations were performed by placing two-dimensional regions of interest (ROIs) on sequential axial slices, around the major coronary arteries including left circumflex (LCx), left main (LM), left anterior descending (LAD), and right coronary artery (RCA). The segmented structures were converted into binary masks in NIfTI format using Plastimatch (Version 0.4.3).

PET normalisation

PET images were converted to SUV normalised to the patient’s body weight. Voxel intensities of the PET image were further normalised by dividing each voxel value by the SUV_{mean} of the blood pool (from the right atrium) prior to feature extraction (see Supplementary Methods) [13]. Radiomic features derived

from voxel-normalised [^{18}F]NaF PET images for both patient- and artery-level analyses are reported. Analyses of non-normalised features are reported in the Supplementary Methods and Results.

Feature extraction

Feature extraction was performed at both patient and arterial levels from both non-normalised and voxel-normalised PET images using the PyRadiomics library (Version 3.0.1), which implements feature calculation in alignment with the Image Biomarker Standardisation Initiative (IBSI) guidelines [14]. A total of 93 radiomic features were extracted from each coronary artery without post processing filters, excluding shape features. These included first-order statistics (n = 18), and various texture features, such as grey level co-occurrence matrix (GLCM, n = 24), grey level dependence matrix (GLDM, n = 14), grey level run length matrix (GLRLM, n = 16), grey level size zone matrix (GLSZM, n = 16), and neighbourhood grey tone difference matrix (NGTDM, n = 5). Detailed IBSI reporting guidelines are presented in Supplementary Tables S1-S3. Individual radiomic features are described in Supplementary Table S4.

CCS progression interpretation

CCS progressor was defined as a change in square root-transformed CCS greater than 2.5 for per-patient analysis and greater than 1.25 for per-coronary analysis, based on established thresholds that account for measurement variability [19, 20]. Further details on analyses utilising alternative thresholds are provided in Supplementary Figure S1.

Conventional PET analysis

The conventional per-coronary approach utilised artery-specific TBR_{max} thresholds [6] to classify arteries with values above the threshold as PET-positive. These were compared between progressing and non-progressing arteries, and precision, recall, and F1 scores were calculated to assess the validity of the dichotomous thresholds. The conventional per-patient approach summarised the number of PET-positive coronary arteries (0–4) [6], reported as proportions across the cohort. The distribution of progressing and non-progressing patients across each category of PET-positive arteries was examined.

Furthermore, the TBR_{max} was assessed as a continuous variable from each coronary artery, and the entire coronary tree. Given the routine use of this measure in vascular PET analyses, this was used as a conventional standard for comparison with radiomic analyses. Building upon this conventional framework, single-feature logistic regression models evaluated whether individual radiomic features outperformed TBR_{max}, while multi-feature models assessed whether combining radiomic features improved predictive performance beyond both TBR_{max} and the baseline CCS. These analyses aimed to determine whether radiomics offers enhanced predictive performance for CCS progression.

Prediction modelling

To assess predictors of CCS progression, CCS, TBR_{max}, radiomics features, and clinical parameters were evaluated using both single-feature and multi-feature logistic regression models. Multi-feature models used logistic regression with least absolute shrinkage and selection operator [21] regularisation [22]. Model development included hyperparameter optimisation via randomised search within a five-fold cross-validation framework. Feature scaling was applied within each fold to prevent data leakage. Multi-feature models were tested across various input configurations, including individual and combined data sources from voxel-normalised and non-normalised PET radiomics, clinical parameters (Table 1), and CCS. The time interval between CT CCS scans was accounted for as a model input, with inclusion determined by LASSO regularisation. Model performance was evaluated using ROC-AUC (Area Under the Receiver Operating Characteristic Curve), precision, recall, and F1 score, with 95% confidence intervals (CI) estimated from 1,000 patient-level bootstrap samples [23]. As ROC-AUC, a threshold-independent metric, may underestimate performance in the presence of class imbalance, PR (Precision-Recall)-AUC was also reported alongside. Comparative analysis of single-feature and multi-feature models was performed based on cross-validation metrics and their 95% CIs. Feature importance methods and results are provided in the Supplementary Figure S2. Sensitivity analyses stratified models by statin use (Supplementary Materials).

Table 1
Patient Characteristics

Patient Population (n = 91)	
Female sex, n (%)	26 (28.6)
Antihypertensives, n (%)	66 (72.5)
Statins, n (%)	67 (73.6)
Antiplatelets, n (%)	32 (35.2)
Insulin, n (%)	26 (28.6)
Vascular disease History, n (%)	9 (9.9)
Smoking History, n (%)	39 (42.9)
Age (years), median [25th to75th percentile]	66 [60–70]
BMI Baseline, median [25th to75th percentile]	29.8 [26.6–32.8]
EGFR mL/(min·1.73 m2), median [25th to75th percentile]	86.0 [76.0–90.0]
Cholesterol (mmol/L), median [25th to75th percentile]	4.1 [3.6–4.8]
Triglyceride (mmol/L), median [25th to75th percentile]	1.6 [1.3–2.3]
HDL cholesterol (mmol/L), median [25th to75th percentile]	1.1 [1.0–1.3]
LDL cholesterol (mmol/L), median [25th to75th percentile]	2.0 [1.6–2.7]
CRP (mg/L), median [25th to75th percentile]	1.8 [1.0–3.8]
Diabetes duration (years), median [25th to75th percentile]	11 [5.0–20.0]
HbA1c (%), median [25th to75th percentile]	7.1 [6.6–7.9]
CCS Baseline (patient level), median [25th to75th percentile]	218 [91–609]
CCS Follow-up (patient level), median [25th to75th percentile]	398 [178–1,018]
Time interval between CCS scans (years), median [25th to75th percentile]	3.1 [2.8–3.4]

BMI = body mass index, eGFR = estimated glomerular filtration rate, HDL = high-density lipoprotein, LDL = low-density lipoprotein, CRP = C-reactive protein, HbA1c = glycated haemoglobin, CCS = coronary calcium score

Results

Patient Characteristics

From 154 participants in the original VIKCOVAC study, 91 were included in this analysis (Fig. 1). The characteristics of the 91 patients included in this study are summarised in Table 1. The majority of the

cohort was male, comprising 71.4% (65/91) of the participants. The median age of the cohort was 66 years (25th to 75th percentile: 60–70). The cohort had a median total baseline CCS of 218 (25th to 75th percentile: 91–609) and a median total follow-up CCS of 399 (25th to 75th percentile: 179–1,018). The median duration of time between CT CCS was 3.1 (25th to 75th percentile: 2.8–3.4) years.

Per-coronary analysis

A total of 211 coronary arteries (58.0%) demonstrated CCS progression over the follow-up period, as presented in Fig. 2. In predicting CCS progression, baseline CCS yielded an ROC-AUC of 0.70 (95% CI: 0.63–0.77), and the TBR_{max} yielded an ROC-AUC of 0.64 (95% CI: 0.58–0.70). Using the dichotomised TBR_{max} thresholds [6], classification performance yielded a similar ROC-AUC of 0.63 (95% CI: 0.58–0.67). Additional metrics such as sensitivity, specificity, precision, and recall are detailed in Table 2. Alternative threshold for CCS progression as described in Supplementary Figure.S1.

Table 2

Performance of Single- and Muti-feature Models Summary of median AUC, F1 score, precision, recall, and corresponding 95% confidence intervals for conventional clinical variables, baseline CCS, TBR_{max}, dichotomous TBR_{max} threshold [6] and the top-performing voxel-normalised radiomic features, alone and in combination.

Model	ROC-AUC	F1	Precision	Recall
Single-feature - Per artery				
Baseline CCS	0.70 (0.63–0.77)	0.74 (0.58–0.79)	0.61 (0.55–0.79)	1.00 (0.47–1.00)
TBR_{max}	0.64 (0.58–0.70)	0.72 (0.62–0.79)	0.62 (0.57–0.67)	0.88 (0.65–1.00)
First Order Total Energy	0.72 (0.66–0.76)	0.73 (0.64–0.80)	0.71 (0.65–0.77)	0.74 (0.59–0.93)
First Order Energy	0.71 (0.65–0.76)	0.73 (0.62–0.80)	0.69 (0.62–0.75)	0.76 (0.56–0.98)
Gray Level Run Length Matrix (GLRLM) Long Run High Gray Level Emphasis	0.69 (0.64–0.74)	0.74 (0.62–0.80)	0.69 (0.63–0.74)	0.80 (0.58–0.96)
GLRLM Run Entropy	0.69 (0.64–0.74)	0.75 (0.67–0.80)	0.67 (0.61–0.73)	0.85 (0.74–0.90)
First Order Range	0.69 (0.64–0.74)	0.74 (0.64–0.80)	0.67 (0.61–0.72)	0.83 (0.67–0.93)
Single-feature - Per patient				
Baseline CCS	0.58 (0.32–0.78)	0.86 (0.85–0.86)	0.75 (0.74–0.76)	1.00 (0.97–1.00)
HbA1c%	0.65 (0.39–0.78)	0.86 (0.83–0.87)	0.75 (0.74–0.79)	1.00 (0.93–1.00)
Baseline BMI	0.56 (0.35–0.71)	0.86 (0.83–0.86)	0.75 (0.74–0.76)	1.00 (0.96–1.00)
eGFR mL/ (min·1.73 m2)	0.55 (0.33–0.70)	0.86 (0.83–0.87)	0.75 (0.74–0.80)	0.99 (0.93–1.00)
TBR_{max}	0.83 (0.73–0.92)	0.86 (0.83–0.91)	0.82 (0.76–0.89)	0.91 (0.87–0.97)
First Order 90th Percentile	0.80 (0.69–0.89)	0.86 (0.82–0.90)	0.81 (0.75–0.87)	0.93 (0.88–0.97)
First Order Root Mean Squared	0.80 (0.69–0.89)	0.86 (0.83–0.90)	0.80 (0.75–0.86)	0.93 (0.88–0.97)
First Order Mean	0.80 (0.68–0.88)	0.86 (0.83–0.90)	0.80 (0.75–0.85)	0.93 (0.88–0.99)

Model	ROC-AUC	F1	Precision	Recall
Single-feature - Per artery				
First Order 10th Percentile	0.75 (0.62–0.86)	0.85 (0.82–0.90)	0.78 (0.74–0.86)	0.93 (0.90–0.97)
First Order Median	0.75 (0.61–0.85)	0.85 (0.82–0.89)	0.78 (0.74–0.84)	0.94 (0.88–1.00)
Multi-feature - Per artery				
CCS + TBR_{max}	0.67 (0.60–0.73)	0.72 (0.62–0.79)	0.65 (0.59–0.72)	0.80 (0.61–0.99)
PET Radiomics	0.75 (0.68–0.82)	0.76 (0.68–0.83)	0.74 (0.65–0.81)	0.79 (0.69–0.89)
Baseline CCS + PET Radiomics	0.77 (0.70–0.83)	0.77 (0.71–0.84)	0.75 (0.67–0.82)	0.80 (0.71–0.89)
Multi-feature - Per patient				
Clinical Features	0.72 (0.54–0.86)	0.85 (0.79–0.91)	0.81 (0.74–0.90)	0.90 (0.79–1.00)
Baseline CCS + Clinical Features	0.72 (0.55–0.86)	0.86 (0.79–0.92)	0.81 (0.74–0.91)	0.90 (0.79–1.00)
CCS + TBR_{max}	0.83 (0.72–0.92)	0.87 (0.83–0.92)	0.82 (0.76–0.89)	0.93 (0.88–0.97)
CCS + TBR_{max} + Clinical Features	0.88 (0.77–0.97)	0.90 (0.85–0.96)	0.88 (0.75–0.96)	0.94 (0.85 -1.00)
PET Radiomics	0.90 (0.80–0.97)	0.91 (0.85–0.96)	0.90 (0.76–0.97)	0.93 (0.87–1.00)
PET Radiomics + Baseline CCS + Clinical Features	0.91 (0.82–0.98)	0.92 (0.86–0.96)	0.91 (0.76–0.97)	0.94 (0.87–1.00)
Dichotomous Threshold - Per artery				
TBR_{max} dichotomous Threshold	0.63	0.54	0.78	0.41

CCS = coronary calcium score, TBR_{max} = maximum target-to-background ratio, GLRLM = gray level run length matrix, HbA1c = glycated hemoglobin, BMI = body mass index, eGFR = estimated glomerular filtration rate.

Note: Several first-order statistics (e.g., mean, median, percentiles, RMS, and range) are often highly correlated, and feature selection methods such as LASSO was used in multi-feature model to reduce redundancy.

Among radiomics features, the most predictive single-feature for CCS progression was first-order total energy (ROC-AUC: 0.72, 95% CI: 0.66–0.76), followed by first-order energy (ROC-AUC: 0.71, 95% CI: 0.65–0.76). The multi-feature model combining baseline CCS and TBR_{max} yielded an ROC-AUC of 0.67 (CI:

0.60–0.73). The multi-feature model using PET radiomics, which included TBR_{max}, demonstrated the highest performance with an ROC-AUC of 0.77 (95% CI: 0.70–0.84), representing a significant improvement ($p < 0.001$) over models using TBR_{max} or baseline CCS alone. The addition of baseline CCS to the PET radiomics multi-feature model did not result in further performance gains (ROC-AUC: 0.77, 95% CI: 0.70–0.83, $p > 0.05$ for comparison of ROC-AUCs). Performance metrics for individual features are summarised in Table 2. Comparison of model ROC-AUCs and their corresponding 95% CI are presented in Table 2 and Fig. 3.

Per-patient analysis

A total of 68 patients (74.7%) demonstrated CCS progression at the patient level. For the prediction of CCS progression HbA1c% achieved the highest ROC-AUC at 0.65 (95% CI: 0.39–0.78) amongst all clinical variables from Table 1. Baseline CCS achieved high recall (1.00, 95% CI: 0.97–1.00) and moderate precision (0.75, 95% CI: 0.74–0.76), reflected in a PR-AUC of 0.77 (95% CI: 0.65–0.90), although the ROC-AUC was lower at 0.58 (95% CI: 0.32–0.78) due to class imbalance and overlapping probability distributions. TBR_{max} demonstrated excellent predictive capabilities, with a median ROC-AUC of 0.83 (95% CI: 0.73–0.92). TBR_{max} was also the most predictive among radiomic features, followed by first-order 90th percentile (ROC-AUC: 0.80, 95% CI: 0.69–0.89). While CI overlapped, TBRmax showed significantly better performance than the other top radiomic features ($p < 0.05$) (Table 2). The overall top performing features are demonstrated in Fig. 4b). Univariate and multivariate regression models are described in Supplementary Table S4 and full feature importance rankings and the top contributing features from the multi-feature model are shown in Supplementary Figure S2.

In multi-feature models, the combination of clinical variables and baseline CCS achieved an ROC-AUC of 0.72 (95% CI: 0.55–0.86). The addition of TBR_{max} in this model significantly enhanced performance, yielding an ROC-AUC of 0.88 (95% CI: 0.77–0.97; $p < 0.05$). A multi-feature model incorporating PET radiomic features, which included TBR_{max}, achieved superior predictive performance (ROC-AUC: 0.90, 95% CI: 0.80–0.97), over the model combining clinical variables, baseline CCS and TBR_{max} ($p < 0.001$). The addition of clinical features and baseline CCS to the PET radiomics model yielded a marginal increase in performance compared with the radiomics multi-feature model alone (ROC-AUC: 0.91, 95% CI: 0.82–0.98, $p < 0.05$) (Table 2, Fig. 4).

Non-normalised PET feature analyses were less predictive of CCS progression than the voxel-normalised analyses, with full results in Supplementary Figures S2-S5. In a sensitivity analysis, there was no significant difference in radiomics models in people being treated with, and not being treated with, statin therapy (supplementary material, and Supplementary Figure S6). Odds radio analysis are presented in Supplementary Tables S5-S7.

Discussion

In this post-hoc analysis of a primary prevention cohort of people with diabetes mellitus, we observed that baseline [^{18}F]NaF activity on PET predicts subsequent CCS progression when measured using traditional analysis methods (TBR_{max}). We describe robust approach to applying radiomics analyses in the examination of coronary PET, and radiomics models improved prediction of CCS progression when compared with the TBR_{max}, baseline CT CCS, and clinical variables. These findings highlight the promising utility of a radiomics approach to coronary PET analyses, and in the context of [^{18}F]NaF PET, demonstrate the predictive capabilities of radiomics over traditional analytical methods in CCS progression.

Radiomics models improved prediction of CCS progression compared with TBR_{max} and baseline CCS, supporting the value of quantitative [^{18}F]NaF PET assessment in this cohort. Only one other study has examined the utility of radiomics in coronary [^{18}F]NaF PET. In a cohort of 293 patients with established coronary artery disease, CMA predicted fatal or non-fatal myocardial infarction with an AUC of 0.76 [24]. In the present study, PET-derived signal performed exceptionally well for discriminating subsequent CT-detected CCS progression, and adding clinical variables and baseline CCS did not provide incremental value, suggesting that radiomics captured most of the discriminative information beyond traditional measures of risk.

Radiomics has been increasingly explored across cardiovascular imaging modalities beyond [^{18}F]NaF PET (CT CCS [25], CTA [26], MRI [27] and [^{18}F]FDG [28]), where radiomic features have been demonstrated discriminative capabilities beyond traditional measures for various hard clinical outcomes or surrogate measures of clinical outcomes. Despite these advances, there has been limited uptake of radiomics in clinical practice, possibly due to only modest improvements of radiomics models over established methods of disease quantification and prognostication. In our study, the radiomics model of [^{18}F]NaF PET was superior to clinical and CT CCS models (ROC-AUC: 0.91, 95% CI: 0.82–0.98 v 0.72. 95% CI: 0.55–0.86, $p < 0.05$) for predicting patient level CCS progression. Coronary PET imaging continues to advance through improved scanner sensitivity, motion correction tools, and the development of more plaque-specific radiotracers. In the continued absence of an agreed upon method of coronary PET analysis and quantification, radiomics may present a promising approach for a prognostically important and standardised assessment of coronary PET signal.

In this cohort, [^{18}F]NaF uptake was strongly predictive of CCS progression. Prior work has linked coronary [^{18}F]NaF activity to clinically meaningful endpoints, supporting the broader prognostic plausibility of this imaging signal. In a 704-patient post-myocardial-infarction cohort, prevalent CMA ([^{18}F]NaF activity at baseline) was independently associated with cardiac death or non-fatal myocardial infarction (HR 1.82, 95% CI: 1.07–3.10; $p = 0.03$) and all-cause mortality (HR 2.43, 95% CI: 1.15–5.12; $p = 0.02$) [8]. Furthermore, [^{18}F]NaF PET has demonstrated independent prognostic utility for CCS progression, a reliable surrogate for CVD risk [19]. In a study of 183 patients with multivessel coronary atherosclerosis, coronary segments with CMA on [^{18}F]NaF PET (TBR_{max} threshold 1.25) progressed in

CCS over 12 months, whereas segments without CMA did not [7]. Mechanistically, [^{18}F]NaF binding depends on hydroxyapatite surface area and local delivery of radiotracer [29], associates with histomorphometric indices of bone turnover [30] and [^{18}F]NaF–avid plaques show microscopic calcification, inflammation, and cholesterol crystals on high-resolution invasive imaging. While our findings indicate that radiomics could strengthen the value of [^{18}F]NaF PET for identifying CCS progression, future work should test whether these radiomic measures improve prediction of definitive clinical endpoints.

This study has several limitations. The analyses were post hoc and based on a modest sample size, limiting generalisability and the ability to assess long term clinical outcomes such as myocardial infarction or death. This study's radiomic analyses lack external validation and are influenced by image preprocessing parameters, segmentation variability, and possible unconsidered clinical confounders. The most predictive single feature was TBR_{max}, a traditional PET metric, underscoring that incremental gains from multi-feature models require rigorous confirmation. These limitations highlight the need for prospective, adequately powered studies with external validation, harmonised pipelines, extended follow up, and clinical outcome data. Loss to follow-up for repeat CCS may have introduced selection bias if follow-up was non-random. This cohort comprised individuals with diabetes mellitus, which restricts translation to broader populations. Nonetheless, the present work advances coronary PET, and specifically [^{18}F]NaF, quantification by demonstrating that multi feature radiomic modelling can augment predictive performance for CCS progression, a surrogate imaging endpoint that has been linked to definitive clinical endpoints.

Conclusions

Radiomics analyses can be reliably applied to the analysis of coronary [^{18}F]NaF PET, where it provides improvement in prediction performance for CCS progression compared with conventional clinical, PET and CT measures. Future research is needed to understand whether radiomics analyses can demonstrate similar prognostic benefits in other radiotracers used in coronary PET imaging, or whether radiomics can improve prediction of CVD events in studies using [^{18}F]NaF PET.

Abbreviations

- CCS: coronary calcium score
- TBR_{max}: maximum target-to-background ratio
- PET: positron emission tomography
- AUC: area under the ROC curve
- CT: computed tomography

Declarations

Ethics approval and consent to participate

This study was a post-hoc analysis of the ViKCoVaC trial, a double-blind 2 × 2 factorial randomised placebo-controlled trial investigating the effect of vitamin K1 and colchicine on arterial calcification activity measured using [^{18}F]NaF PET. The trial was registered with the Australian New Zealand Clinical Trials Registry (ACTRN12616000024448) and was approved by the Royal Perth Hospital Human Research Ethics Committee (REG14-095) on 30/09/2014. Written informed consent was obtained from all participants.

Consent for publication

Written informed consent was obtained from all participants.

Availability of data and materials

The datasets generated and/or analysed during the current study are not publicly available due to participant privacy, ethical restrictions and institutional data governance requirements. Data may be available from the corresponding author on reasonable request, subject to appropriate ethical approval and institutional data-sharing agreements.

Competing interests

The authors declare that they have no competing interests.

Funding

This research was supported by a grant from the Royal Perth Hospital Research Foundation, with additional support from the Research and Training Program at the University of Western Australia, the Charlies Foundation for Research, the UWA Data Institute, and the UWA Medical Physics Machine Learning Cluster.

Authors' contributions

SL, JB, CS, JK, MAE contributed to study conception and design. CS, SCL, JB, RF contributed to participant recruitment, clinical data collection and imaging acquisition. SL performed image processing; JB and SCL performed coronary segmentation; SL performed radiomic feature extraction and statistical analysis. SL, NB, GMH and JK contributed to interpretation of the results. SL drafted the manuscript. All authors critically revised the manuscript, read and approved the final manuscript, and agree to be accountable for all aspects of the work.

Acknowledgements

The authors thank the participants of the ViKCoVaC trial and the clinical, imaging and research staff involved in recruitment, imaging and study coordination.

Authors' information

Not applicable.

References

1. Detrano R, et al. Coronary calcium as a predictor of coronary events in four racial or ethnic groups. N Engl J Med. 2008;358(13):1336–45. 10.1056/NEJMoa072100.
2. Lehmann N, et al. Value of Progression of Coronary Artery Calcification for Risk Prediction of Coronary and Cardiovascular Events: Result of the HNR Study (Heinz Nixdorf Recall). Circulation. 2018;137(7):665–79. 10.1161/CIRCULATIONAHA.116.027034.
3. Irkle A, et al. Identifying active vascular microcalcification by (18)F-sodium fluoride positron emission tomography. Nat Commun. 2015;6:7495. 10.1038/ncomms8495.
4. Joshi NV et al. *18 F-fluoride positron emission tomography for identification of ruptured and high-risk coronary atherosclerotic plaques: a prospective clinical trial.* The Lancet, 2014. 383(9918): pp. 705–713. 10.1016/S0140-6736(13)61754-7
5. Majeed K, et al. Coronary (18)F-sodium fluoride PET detects high-risk plaque features on optical coherence tomography and CT-angiography in patients with acute coronary syndrome. Atherosclerosis. 2021;319:142–8. 10.1016/j.atherosclerosis.2020.12.010.
6. Bellinge JW et al. *18 F-Sodium Fluoride Positron Emission Tomography Activity Predicts the Development of New Coronary Artery Calcifications.* Arteriosclerosis, Thrombosis, and Vascular Biology, 2021. 41(1): pp. 534–541, doi:10.1161/ATVBAHA.120.315364
7. Doris MK, et al. Coronary (18)F-Fluoride Uptake and Progression of Coronary Artery Calcification. Circ Cardiovasc Imaging. 2020;13(12):e011438. 10.1161/CIRCIMAGING.120.011438.
8. Moss A, et al. Coronary Atherosclerotic Plaque Activity and Future Coronary Events. JAMA Cardiol. 2023;8(8):755–64. 10.1001/jamacardio.2023.1729.
9. Mingels C, et al. Long-axial field-of-view PET/CT for the assessment of inflammation in calcified coronary artery plaques with [(68) Ga]Ga-DOTA-TOC. Eur J Nucl Med Mol Imaging. 2024;51(2):422–33. 10.1007/s00259-023-06435-6.
10. Doris MK, et al. Optimization of reconstruction and quantification of motion-corrected coronary PET-CT. J Nucl Cardiol. 2020;27(2):494–504. 10.1007/s12350-018-1317-5.
11. Keeling GP, et al. Development and validation of an activatable PET radiotracer reporting extracellular myeloperoxidase activity for the detection of unstable atherosclerotic plaque. Npj Imaging. 2026;4(1). 10.1038/s44303-026-00156-9.
12. Tzolos E, et al. Noninvasive In Vivo Coronary Artery Thrombus Imaging. JACC Cardiovasc Imaging. 2023;16(6):820–32. 10.1016/j.jcmg.2022.10.002.
13. Kwiecinski J, et al. Whole-vessel coronary F-sodium fluoride PET for assessment of the global coronary microcalcification burden. Eur J Nucl Med Mol Imaging. 2020;47(7):1736–45.

10.1007/s00259-019-04667-z.

14. Zwanenburg A, et al. The image biomarker standardization initiative: standardized quantitative radiomics for high-throughput image-based phenotyping. Radiology. 2020;295(2):328–38. 10.1148/radiol.2020191145.
15. Capobianco E, Deng J. *Radiomics at a Glance: A Few Lessons Learned from Learning Approaches.* Cancers, 2020. 12(9), doi:ARTN 2453 10.3390/cancers12092453
16. Li S, et al. Auto-segmentation, radiomic reproducibility, and comparison of radiomics between manual and AI-derived segmentations for coronary arteries in cardiac [(18)F]NaF PET/CT images. EJNMMI Phys. 2025;12(1):42. 10.1186/s40658-025-00751-6.
17. Bellinge JW, et al. The effect of Vitamin-K(1) and Colchicine on Vascular Calcification Activity in subjects with Diabetes Mellitus (ViKCoVaC): A double-blind 2x2 factorial randomized controlled trial. J Nucl Cardiol. 2022;29(4):1855–66. 10.1007/s12350-021-02589-8.
18. Agatston AS, et al. Quantification of coronary artery calcium using ultrafast computed tomography. J Am Coll Cardiol. 1990;15(4):827–32. 10.1016/0735-1097(90)90282-t.
19. Budoff MJ, et al. Progression of coronary artery calcium predicts all-cause mortality. JACC Cardiovasc Imaging. 2010;3(12):1229–36. 10.1016/j.jcmg.2010.08.018.
20. Hokanson JE, et al. Evaluating changes in coronary artery calcium: an analytic method that accounts for interscan variability. AJR Am J Roentgenol. 2004;182(5):1327–32. 10.2214/ajr.182.5.1821327.
21. Roth GA, et al. Global, Regional, and National Burden of Cardiovascular Diseases for 10 Causes, 1990 to 2015. J Am Coll Cardiol. 2017;70(1):1–25. 10.1016/j.jacc.2017.04.052.
22. Tibshirani R. *Regression shrinkage and selection via the Lasso.* Journal of the Royal Statistical Society Series B-Statistical Methodology, 1996. 58(1): pp. 267–288, doi:10.1111/j.2517-6161.1996.tb02080.x
23. Riley RD, Collins GS. Stability of clinical prediction models developed using statistical or machine learning methods. Biom J. 2023;65(8):2200302. 10.1002/bimj.202200302.
24. Kwiecinski J, et al. Coronary (18)F-Sodium Fluoride Uptake Predicts Outcomes in Patients With Coronary Artery Disease. J Am Coll Cardiol. 2020;75(24):3061–74. 10.1016/j.jacc.2020.04.046.
25. Eslami P, et al. Radiomics of Coronary Artery Calcium in the Framingham Heart Study. Radiol Cardiothorac Imaging. 2020;2(1):e190119. 10.1148/ryct.2020190119.
26. Kolossvary M, et al. Coronary Plaque Radiomic Phenotypes Predict Fatal or Nonfatal Myocardial Infarction: Analysis of the SCOT-HEART Trial. JACC Cardiovasc Imaging. 2025;18(3):308–19. 10.1016/j.jcmg.2024.08.012.
27. Fahmy AS et al. *Radiomics and deep learning for myocardial scar screening in hypertrophic cardiomyopathy.* Journal of Cardiovascular Magnetic Resonance, 2022. 24(1), doi:ARTN 40 10.1186/s12968-022-00869-x

28. Duff LM, et al. An Automated Method for Artifical Intelligence Assisted Diagnosis of Active Aortitis Using Radiomic Analysis of FDG PET-CT Images. Biomolecules. 2023;13(2). 10.3390/biom13020343.
29. Czernin J, Satyamurthy N, Schiepers C. Molecular mechanisms of bone 18F-NaF deposition. J Nucl Med. 2010;51(12):1826–9. 10.2967/jnumed.110.077933.
30. Piert M et al. Assessment of porcine bone metabolism by dynamic. J Nucl Med, 2001. 42(7): p. 1091 – 100, doi:PMID: 11438633.

Figures

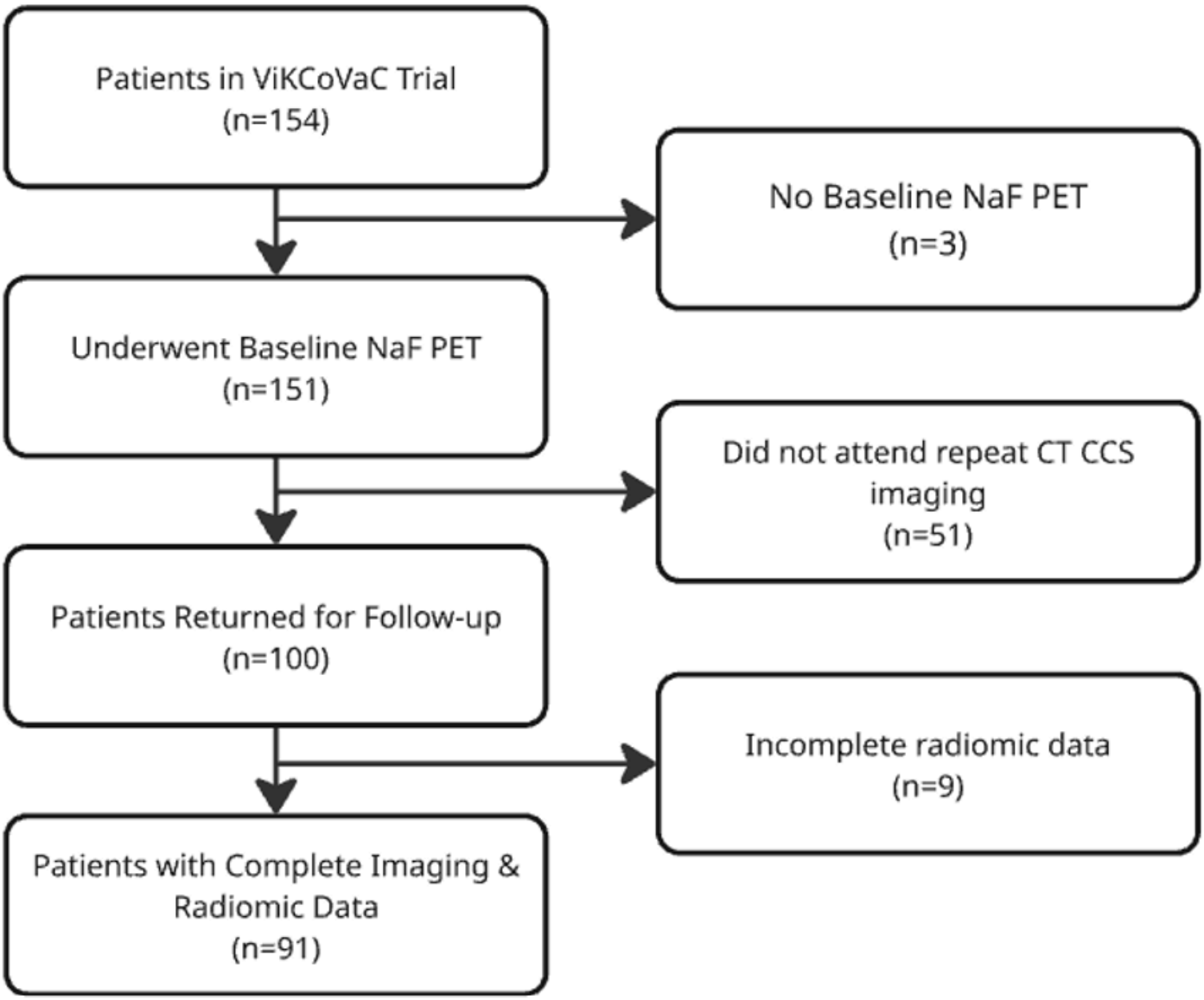


Figure 1

Patient cohort flow diagram. Flow diagram showing participant inclusion from the original VIKCOVAC cohort to the final analytic cohort with baseline [18F]NaF PET/CT and follow-up coronary calcium

scoring. NaF = sodium fluoride; PET = positron emission tomography; CT = computed tomography.

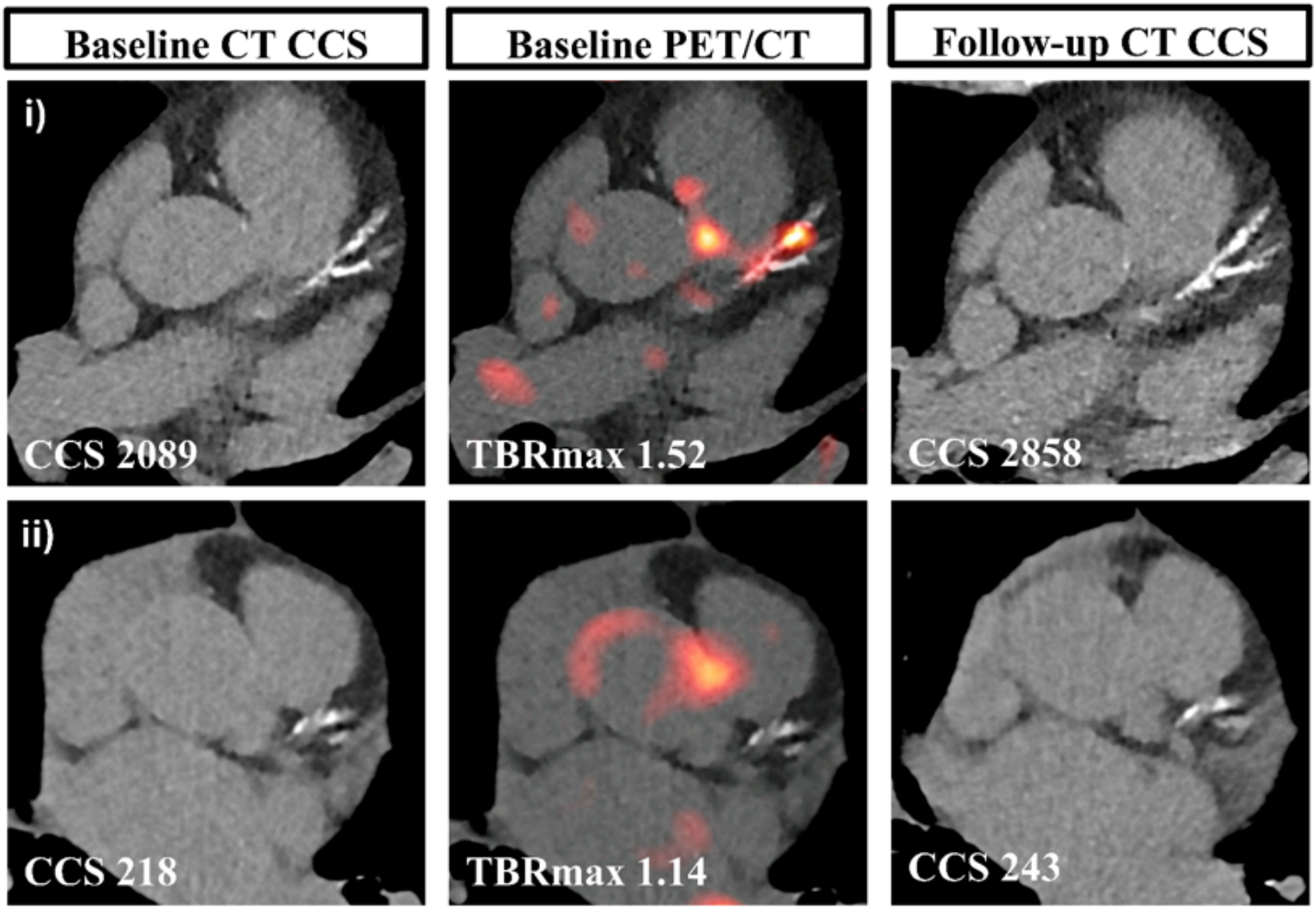


Figure 2

Representative coronary [^{18}F]NaF PET/CT images and CT coronary calcium score progression. Baseline noncontrast CT CCS images (left), fused baseline [^{18}F]sodium fluoride ([^{18}F]NaF) PET/CT images (middle), and follow-up noncontrast CT CCS images (right) in three representative participants. Focal coronary [^{18}F]NaF uptake with elevated maximum target-to-background ratio (TBR_{max}) is shown at baseline, with corresponding interval progression of CT-detected coronary calcification on follow-up imaging. PET images are windowed to highlight coronary [^{18}F]NaF activity (row i: standardized uptake value [SUV], 1.2–1.8; row ii: SUV, 1.8–2.5). CCS = coronary calcium score; CT = computed tomography; NaF = sodium fluoride; PET = positron emission tomography; SUV = standardized uptake value; TBR_{max} = maximum target-to-background ratio.

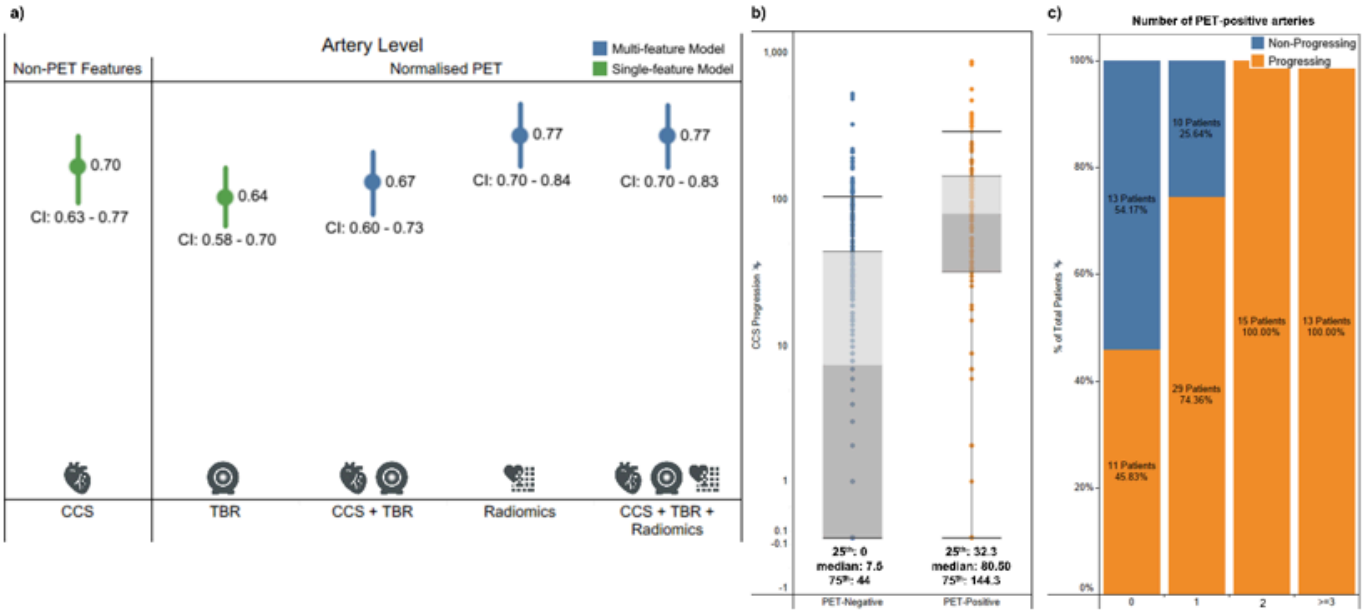


Figure 3

Artery-level analysis of [^{18}F]NaF PET quantification methods.

a) Median ROC-AUC values with 95% confidence intervals from 1000 bootstrap iterations for single- and multi-feature artery-level models. Models included baseline CCS, TBR_{max}, combined CCS + TBR_{max}, PET radiomics alone, and combined CCS + TBR_{max} + PET radiomics. b) Boxplot showing change in CCS from baseline to follow-up in PET-positive and PET-negative arteries. c) Percentage of patients with CCS progression according to the number of PET-positive arteries. CCS = coronary calcium score; NaF = sodium fluoride; PET = positron emission tomography; ROC-AUC = receiver operating characteristic area under the curve; TBRmax = maximum target-to-background ratio.

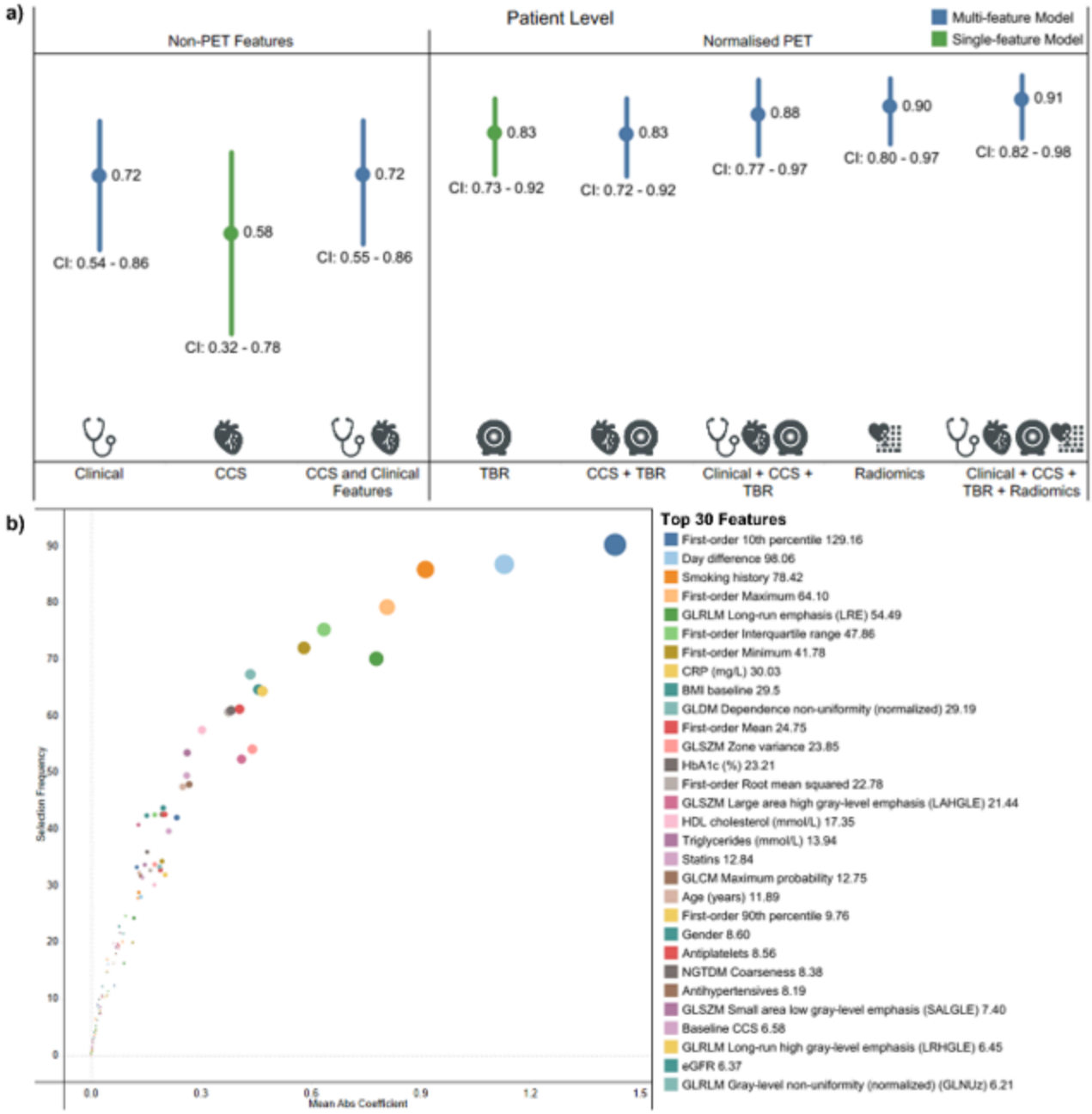


Figure 4

Patient-level analysis of [^{18}F]NaF PET quantification methods.

a) Median ROC-AUC values with 95% confidence intervals from 1000 bootstrap iterations for single- and multi-feature patient-level models. Models without PET features included clinical features alone, CCS alone, and combined clinical features + CCS. Models incorporating PET features included TBR_{max} alone, combined CCS + TBR_{max}, combined clinical features + CCS + TBR_{max}, PET radiomics alone, and combined clinical features + CCS + TBR_{max} + PET radiomics. All PET-based models used voxel-normalised PET features. b) Scatter plot showing feature importance for the combined clinical and PET radiomics multi-feature model. The x-axis represents the mean absolute coefficient for features

assigned a non-zero coefficient during bootstrap iterations, and the y-axis represents selection frequency, defined as the proportion of bootstrap iterations in which each feature received a non-zero coefficient. Circle size represents the feature importance score, calculated as the product of mean absolute coefficient and selection frequency. Numbers in the legend indicate the calculated importance scores. CCS = coronary calcium score; NaF = sodium fluoride; PET = positron emission tomography; ROC-AUC = receiver operating characteristic area under the curve; TBRmax = maximum target-to-background ratio.

Supplementary Files

This is a list of supplementary files associated with this preprint. Click to download.

- CardiacNaFPETSUPP.docx
- CardiacNaFSTARD2015Checklist.docx